Matteo Colombo
Paolo Martinelli*
Marco di Prisco

A design approach for tunnels exposed to blast and fire

1 Introduction

The use of steel fibre-reinforced concrete (SFRC) for partial or total substitution of the traditional steel bar reinforcement in precast tunnel segments is a promising solution that has attracted growing interest over the last few years. Several advantages characterize the SFRC solution compared with the conventional reinforced concrete (RC) one: improved durability plus higher fatigue, fire and impact resistance. The very high toughness is also crucial in two other construction phases: during handling operations and when the tunnel boring machine (TBM) advances by pushing the lining by means of hydraulic jackets. At the serviceability loading condition, segmental circular tunnel linings are mainly subjected to normal forces combined with relatively low bending moments. This particular loading condition suggests the use of SFRC segments with minimum reinforcement just to guarantee robustness requirements. Several SFRC segment applications with a low percentage of conventional reinforcement have been reported in the literature. Nevertheless, the blast load situation in the lining design has not been investigated so far. In the case of a confined environment, as with an internal explosion in a tunnel, the explosive energy density is amplified compared with that of an unconfined blast, making tunnels particularly sensitive to such a load scenario. Explosions are, in many cases, the extreme consequence of fire accidents.

Tunnel linings have been studied in the past with FE models of differing complexity, apart from analytical and empirical methods [1]. The FE models can be two- or three-dimensional; in the former they are built up with beam [2–4] or plane stress elements [5–7], in the latter characterized by having shell or solid brick elements [1, 5, 8]. Concrete and soil materials are generally considered as elastic, but in some cases they are treated as non-linear; rotating and fixed smeared crack approaches, based on fracture energy, were adopted to model the concrete material by *Cavalaro* et al. [6] and *Arnau* & *Molins* [5] respectively, whereas a smeared crack approach formulated within the framework of the theory of plasticity was adopted by *Winkler* et al. [7].

Three-dimensional FE models are still confined to the research field and are rarely adopted in common practice. The FE approach proposed here is intended to be a simplified procedure that is completely accessible to designers so they can investigate the robustness and, in particular, study the behaviour and safety of underground tunnels for the case of internal explosion and pre-explosion fire actions.

The tunnel geometry considered is that adopted for the metro line in Brescia, Italy. The FE model is tested under static serviceability loads. Once the model has been tested, several dynamic analyses are carried out in order to reproduce the blast scenario. The aim of this work is to generate pressure-impulse (*p-i*) diagrams for underground tunnels for the case of internal explosion possibly preceded by fire accident.

The *p-i* diagrams represent a common design tool used to establish the safe response limits induced by blast loads [9–10]. Generating *p-i* diagrams for structures or

* Corresponding author: paolo.martinelli@polimi.it

Submitted for review: 30 June 2014
Revised: 28 August 2014
Accepted for publication: 05 September 2014

structural components is often based on the simplified single-degree-of-freedom (SDOF) model. A rigid-plastic beam based on closed-form solutions was derived for assessing buried structures for the case of internal [11] and external [12] blast loads. However, these studies were limited to buried structures with a rectangular cross-section.

The limit state (or damage) criterion necessary for generating *p-i* diagrams is generally defined in terms of a displacement or deformation response. A new limit state criterion based on the ultimate eccentric flexural capacity (*M-N* interaction diagram) is introduced in this work. Moreover, the criterion takes into account fire-blast interaction thanks to a proper modification of the *M-N* diagram. An innovative layered tunnel segment structural solution made of different fibre-reinforced cementitious composites, recently proposed by *di Prisco* et al. [13], is compared with a traditional RC solution. In particular, the aim of the paper is to generate *p-i* diagrams for the two solutions investigated considering the tunnel exposed to a hydrocarbon fire scenario before the explosion. Several fire exposure times (t = 0, 60, 120, 180 min) are considered for the discussion of the proposed design procedure, and the performance of the two structural solutions is compared for static and dynamic loads.

2 Tunnel geometry

Brescia is a city with about 200 000 inhabitants in the northern part of Italy (Lombardy region). The Brescia metro line consists of a single line 13.7 km long, with 17 stations from Buffalora to Prealpino characterized by platform edge doors. Construction work started in April 2003 and the line was finished in March 2013. The lining has an internal diameter of 8.15 m and a thickness of 350 mm. The tunnel design depth projection, measured from the centre-line of the lining, is about 23.12 m, with a tunnel overburden of 18.7 m. The lining is composed of six precast segments and a smaller key segment (6+1), having an average width of 1500 mm. A transverse section through the Brescia metro lining is shown schematically in Fig. 1.

3 Tunnel structural solutions and materials

The tunnel lining structural solution adopted as a reference case is made of RC material with class C40 plain concrete and steel reinforcement with a characteristic yield stress f_{yk} = 430 MPa.

The second structural solution proposed here is the SFRC layered segment solution. A two-layer segment with an intrados skin made of high-performance fibre-reinforced cementitious composite (HPFRCC) and a core filled by SFRC is considered in this study (Fig. 2). The solid SFRC core is partially reinforced with two light circumferential cages of conventional reinforcement, mainly introduced to suit the demoulding phase safety checks and to resist the stretching action due to jack pushing during excavation. The segment cross-sections for both the RC and the layered fibre-reinforced solutions are shown in Fig. 3. The figure only shows the longitudinal reinforcement for the two solutions considered. It is important to point out that the reference RC solution also included a certain amount of transverse reinforcement (transverse reinforcement ratio ρ_t = 0.2 %). Examples of fibre-reinforced materials with characteristics similar to those adopted in this study can be found in recent studies [13–14]. *Colombo* et al. [14] carried out shock tube experiments with reflect-

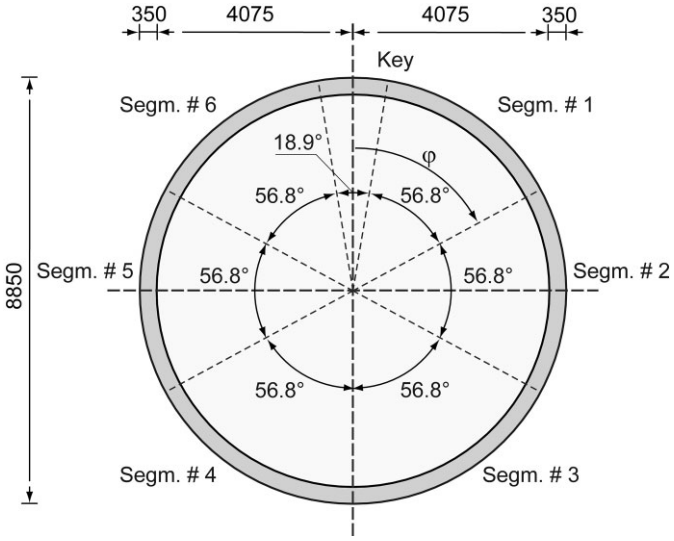

Fig. 1. Section through Brescia tunnel lining (dims. in mm)

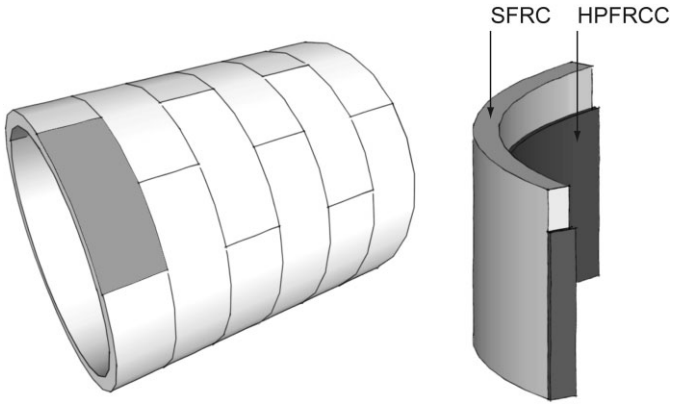

Fig. 2. Stratigraphy investigated for the new layered precast tunnel segment lining

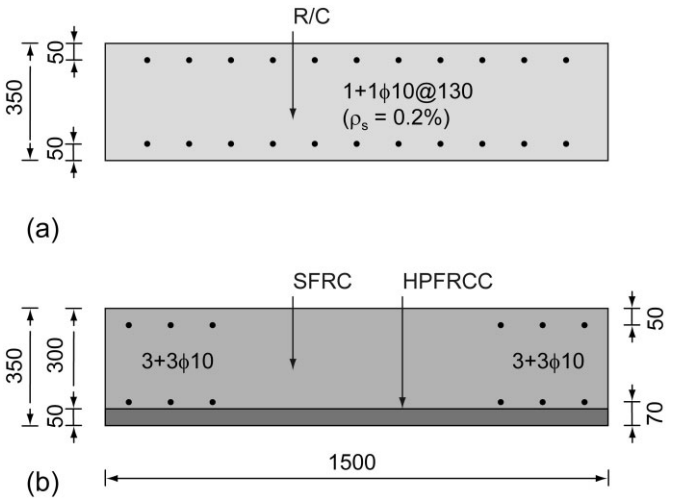

Fig. 3. Tunnel segment cross-sections: a) traditional RC solution and b) innovative fibre-reinforced layered solution (dims. in mm)

Table 1 Material classification and properties at room conditions (f_{ck} = cylinder characteristic compressive strength, f_{R1} = characteristic residual strength @ CMOD = 0.5 mm, f_{R3} = characteristic residual strength @ CMOD = 2.5 mm, CMOD = crack mouth opening displacement, K = fibre orientation factor)

Property	Material		
	SFRC	HPFRCC	Plain concrete
Compressive class	C60	C110	C40
f_{ck} (N/mm^2)	60	110	40
Tensile class	5c	15b	–
f_{R1k} (N/mm^2)	5.0	15	–
f_{R3k}/f_{R1k} (–)	0.9	0.7	–
f_{R3k} (N/mm^2)	4.5	10.5	–
K (–)	1.0	0.64	–
f_{R3k}/K (N/mm^2)	4.5	16.5	–

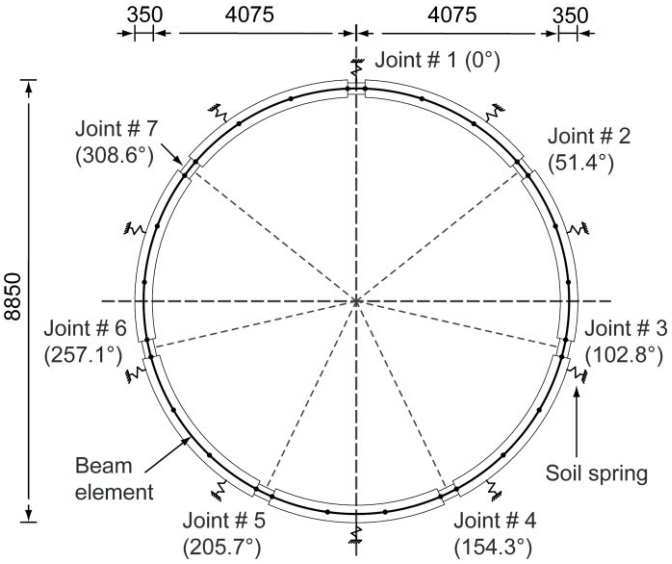

Fig. 4. Schematic layout of the FE model for a single ring (dims. in mm)

ed pressures up to 1 MPa and specific impulses up to about 10 MPa · ms in order to investigate a small portion of tunnel segment interacting with soil subjected to a plane shock wave. The aim of such experimental work was to study the effect of impulse-like distributed pressure over tunnel rings under blast loads in order to develop this new layered precast tunnel segment made of different fibre-reinforced cementitious composites. The study revealed that the reflection of the shock wave between the different layers and the reflection between specimen and soil did not cause any delamination or detachment.

SFRC and HPFRCC are characterized by a compressive class equal to C60 and C110 respectively (Table 1). The tensile class for SFRC and HPFRCC is "5c" and "15b" respectively according to the classification in the *fib* Model Code for Concrete Structures 2010 [15]. A favourable fibre orientation factor $K = 0.64$ acting on just the f_{R3} value is considered according to recent experimental tests carried out on thin structural specimens [16]. Table 1 also lists the residual tensile characteristic strengths at several crack opening displacements for both the fibre-reinforced concrete materials.

4 FE model

The FE model adopted in this study is based on a beam model with soil interaction as proposed by *Groeneweg* [3], which combines beam elements and elastic springs. The model developed here consists of three rings lying on three parallel planes orthogonal to the longitudinal tunnel axis. A schematic layout of the FE model is shown in Fig. 4. The rings are discretized with 2-node *Timoshenko* linear beam elements (B31) with six degrees of freedom per node. A linear elastic material, having a *Young*'s modulus of 38 GPa and a *Poisson*'s ratio of 0.25, is adopted for the beam elements. The longitudinal joints represent the connection of the seven segments for each ring, while the ring joints represent the interaction between different rings. The finite element program ABAQUS/Standard 6.12 [17] was used for all the numerical simulations.

The model adopted in this study differs from the original proposal of *Groeneweg* [3], mainly for two reasons: a) the use of three rings instead of two to simulate better the position of the explosion source, and b) a different treatment of the longitudinal joints to guarantee the joint expansion in the case of internal explosion as described in the following.

The ground-lining interaction is simulated through a simplified approach based on radial linear elastic springs. As in [18], the radial spring stiffness per unit area K_{soil} (subgrade reaction modulus) is estimated according to:

$$K_{soil} = \frac{0.5E_{soil}}{R_{ext}} \tag{1}$$

where E_{soil} is the elastic modulus of the soil and R_{ext} is the external radius of the lining.

The interaction between the three rings is taken into account with shear springs that simulate the ring joints. The approach adopted in this work for the ring spring stiffness estimation is described by *Groeneweg* [3]. *Tiberti* & *Plizzari* [19] carried out a parametric study analysing the influence of the ring shear stiffness on the lining behaviour. A total spring stiffness value for the ring joint $K_v = 1 \times 10^7$ kN/m is assumed in this work as proposed by *Tiberti* & *Plizzari* [20] for the Brescia tunnel lining.

The longitudinal joints can only transfer normal compressive stress. They exhibit a non-linear rotational behaviour that depends on the normal ring force, and that can be simulated by introducing a non-linear rotational spring [21]. *Janßen* [21] proposed a joint where the contact area can be represented by a concrete beam with a width equal to the width of the joint contact area (segmental width) and a depth equal to the joint's contact height. The contact area can have a significant influence on the joint rotational stiffness, as pointed out by *Tiberti* & *Plizzari* [19]; a contact height $h_t = 0$ or 350 mm corresponds to a hinge or a continuum joint configuration respectively. A beam element with a cross-section depth $h_t = 2/3H_{tot} = 233$ mm is assumed for the joints in this study.

The joint elements are modelled with a linear elastic material in compression ($E = 38$ GPa, $\nu = 0.25$) and a no-

Table 2 FE geometric and material characteristics (E = *Young*'s Modulus, ν = *Poisson*'s ratio, k = stiffness)

	# (–)	E (MPa)	ν (–)	k (N/m)
Segment elements	1494	38 250	0.25	–
Joint elements	42	38 250	0.25	–
Nodes	1536	–	–	–
Soil spring	768	–	–	6.44×10^6
Ring-ring joint spring	512	–	–	2.73×10^8
Segment-segment joint spring	21	–	–	1.23×10^9

tension branch. As a consequence, the rotational stiffness of the joint is a function of the axial force acting on the joint itself, and the maximum effective height of the joint is therefore equal to the cross-section depth h_t assigned to the joint element.

Contrasting with the static condition, in the case of an internal tunnel explosion, the lining may be subjected to a tensile force. In many tunnels, a steel rod constitutes the longitudinal joint; it is modelled by an elastic spring that has the same stiffness as the rod. This spring acts in parallel with the joint beam element but, owing to the much smaller stiffness in compression with respect to the joint, it can be neglected when a compressive axial force is acting. On the other hand, this spring allows the lining to expand due to the internal pressure applied.

A summary of the FE mesh characteristics for the model, including the total number of segment and joint elements, total number of nodes, total number of longitudinal joint springs, ring joint springs and soil springs is listed in Table 2. The material characteristics for the beam elements as well as the stiffnesses adopted for the several springs are given in the same table.

5 Static analysis

Before studying the tunnel's structural response to an internal explosion, the FE model was first tested under static serviceability loads. The lining was embedded in a geomechanical group consisting mainly of heterogeneous gravel with the following geotechnical properties: internal friction angle ϕ = 38°, elastic modulus E_{soil} = 350 MPa, density ρ = 20 kN/m^3 and cohesion c = 0 [4]. The soil load condition was simulated by radial pressure, determined according to *Blom* [18], whose magnitude varies along the lining. The distribution of the radial pressure as a function of the angle φ (see Fig. 1) is:

$$\sigma_r(\varphi) = \sigma_{v,eff}\left[\cos^2(\varphi) + k_0 sen^2(\varphi)\right] + \sigma_w(\varphi) \quad (2)$$

where:

$\sigma_{v,eff}$ effective vertical pressure at centre of tunnel
k_0 neutral soil coefficient equal to 0.38
σ_w effective groundwater pressure

For the sake of brevity, the complete geological conditions of the Brescia metro tunnel are omitted here, but they can be found in *Tiberti* [4]. It is worth noting that water pressure is neglected since the water table is below the lower boundary of the lining. Eq. (2) results in a maximum soil pressure of 474 kPa occurring at the top and bottom of the tunnel, whereas the lowest pressure is 182 kPa and occurs at the arch sides.

A parametric study of how a) longitudinal joints, b) ring joints and c) the ground support stiffness influence the ring behaviour was conducted on the Brescia tunnel lining by *Tiberti* & *Plizzari* [19]. The influence of soil spring numbers on the model response was analysed in a previous study by *Colombo* et al. [22]. The number of soil springs can affect the accuracy of the computation results quite significantly. In fact, if the number of springs is not sufficient, the springs behave as discrete supports, modifying the internal action diagrams and the deformed shape.

Fig. 5 shows the bending moment and the shear force diagrams for the FE model with an adequate number of soil springs (256 for each ring). The figure refers to the central ring and shows a maximum external and internal bending moment of about 118 kNm, while the maximum shear force is about 56 kN.

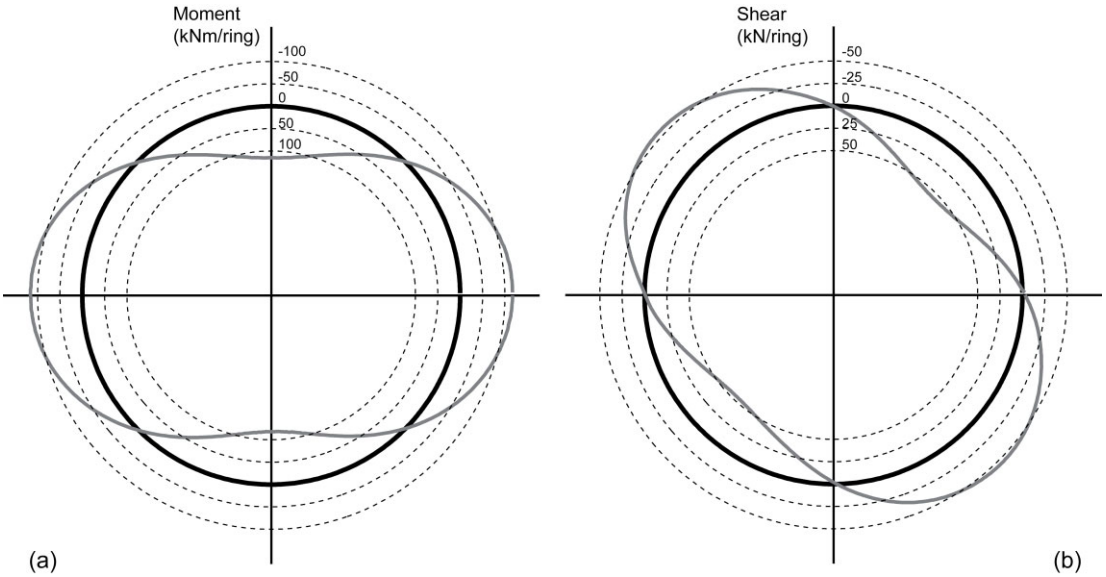

Fig. 5. a) Bending moment and b) shear force diagrams for static loads

6 Integrated approach for tunnels subjected to blast and pre-blast fire actions

The soil pressure is first applied in a static analysis, followed by the dynamic analysis of the model. A safety factor of 1 is used for the dead load according to the *fib* Model Code 2010 suggestion for accidental actions [15]. An implicit time integration scheme is adopted for the dynamic analysis. This choice is due to the fact that spring elements are available in ABAQUS/Standard and not in ABAQUS/Explicit. An explicit time integration scheme based on the central difference integration rule is usually adopted for blast simulations; however, in this study, the sources of non-linearity are small and limited to the joint sections (linear elastic material in compression combined with a no-tension branch). All non-linear time–history analyses adopt the *Hilber-Hughes-Taylor* time integration method, with a minimum time step of 1×10^{-7} s.

The damping ratio assumed for the structure can have a considerable effect on the *p-i* diagram [10]. Damping ratios between 2 and 7 % are normally assumed for RC structures under usual conditions. For cases involving significant external damping, such as the case being studied (soil–structure interaction in an underground tunnel), the damping ratio might well be > 10 % [23]. In this study a *Rayleigh* damping is assumed, with the damping matrix proportional to the mass and initial stiffness matrix. The constants are calibrated to give a damping ratio of 10 % for the first four modes of the structure.

A recent study [24] has shown that in the case of internal tunnel explosions, the pressure distribution does not depend on the tunnel's structural response, thus allowing direct application of a pressure-time history to the structure, while neglecting fluid-structure interaction phenomena.

The excitation pulse shape chosen for all the *p-i* diagrams is a right-angled triangular pulse, which is often used in the literature for representing blast load shape. In this way, maximum pressure p and impulse i unequivocally describe the load history and therefore several simulations for different *p,i* couples have to be run to define the point that generated the *p-i* diagrams. It is worth noting that the blast pressure is applied to the central tunnel ring.

6.1 Limit state definition

The failure criterion considered in this paper refers to the eccentric bending ultimate limit state (ULS) and therefore to the bending moment M vs. axial force N interaction diagrams. No interaction between the transverse and longitudinal bending moments is considered. It is worth noting that, as often happens in ULS design, all the material non-linearities are only considered when computing the cross-section resistance, thus considering the structure as elastic when computing the actions.

In order to take into account the fire-blast interaction, a hydrocarbon fire curve typical of a fire in a tunnel is considered, and the *M-N* diagram for the cross-section is defined for different fire exposure times.

The temperature distribution over the cross-section is computed by means of a 2D finite element heat transfer analysis of the tunnel segment's rectangular cross-section. A hydrocarbon fire curve is imposed at the intrados of the tunnel cross-section. Eq. (3) describes the hydrocarbon fire curve adopted:

$$\theta = 20 + 1080\left[1 - 0.325e^{-0.167t} - 0.675e^{-2.5t}\right] \tag{3}$$

A radiation coefficient h = 15 W/m^{2}K and a convection constant of 0.5 are considered in the model at the intrados surface. Non-linear conduction is considered by adopting conductivity K_C, density ρ and specific heat c_p as a function of temperature θ according to the formulation proposed by Eurocode 2 [25]. The equations representing such parameters are given below:

$$K_C = 2 - 0.24\left(\frac{\theta}{120}\right) + 0.012\left(\frac{\theta}{120}\right)^2 \qquad [\mathrm{W/mK}] \tag{4}$$

$$\rho = \begin{cases} 2300\,[\mathrm{kg/m^3}], & \theta < 100°C \\ 2250\,[\mathrm{kg/m^3}], & \theta \geq 100°C \end{cases} \tag{5}$$

$$c_p = 900 + 80\left(\frac{\theta}{120}\right) - 4\left(\frac{\theta}{120}\right)^2 \qquad [\mathrm{J/kgK}] \tag{6}$$

The numerical results of the thermal analyses are presented in Fig. 6a by means of the temperature history at different points over the cross-section depth, and in Fig. 6b by means of the temperature distribution over the segment cross-section at different fire exposure times.

Temperature distribution over the cross-section is instrumental in the construction of the *M-N* interaction diagrams for the different exposure times considered.

According to the procedure proposed by *fib* Model Code 2010 [15], the *M-N* interaction diagram is defined by evaluating bending moment vs. curvature diagrams for the tunnel cross-section for different axial forces and by considering the peak of each curve as the resistant moment for the given axial force. The bending moment M – curvature χ response is computed by means of a multi-layer plane section approach [26–27].

The compressive behaviour of concrete is defined by a parabola-rectangular constitutive law, whereas an elastic-perfectly plastic constitutive law is adopted for steel reinforcement.

Regarding the uniaxial tensile behaviour of concrete, a tension-free behaviour is used for plain concrete, whereas the linear stress-crack opening constitutive law proposed by *fib* Model Code 2010 [15, 28] is adopted for both of the fibre-reinforced concretes considered. The constitutive laws adopted are illustrated in Fig. 7. According to *fib* Model Code 2010 [15], in the case of fire design, the safety factors for the material strengths are set to 1.

It is worth noting that, since the maximum strain rate achieved during the whole set of analyses is < 1.1 s^{-1}, the dynamic increase factor for material strengths is taken as 1 in favour of safety.

The *M-N* curve is generated by considering 35 different values of axial force ranging between –200 kN (tension) and 24 000 kN (compression) for both positive and negative bending moments. It is worth noting that for the layered solution, the *M-N* diagrams are not symmetrical, even for t = 0 min, due to the lack of symmetry along the horizontal axis of the cross-section. An example of the

M-N construction that refers to the layered solution for $t = 0$ min is shown in Fig. 8.

In order to take into account the fire damage for each layer of the cross-section, the mechanical properties corresponding to the layer temperature are adopted. In particular, the mechanical property decay laws proposed by Eurocode 2 [25] are adopted for concrete compressive strength and steel reinforcement yield strength, whereas for the FRC uniaxial tensile behaviour, the mechanical decay laws detected experimentally by *Colombo* et al. [29] and by *Caverzan* et al. [30] are taken into account for SFRC and HPFRCC respectively (Fig. 9).

A comparison of the *M-N* diagrams for layered and reference solutions for different fire exposure times ($t = 0$,

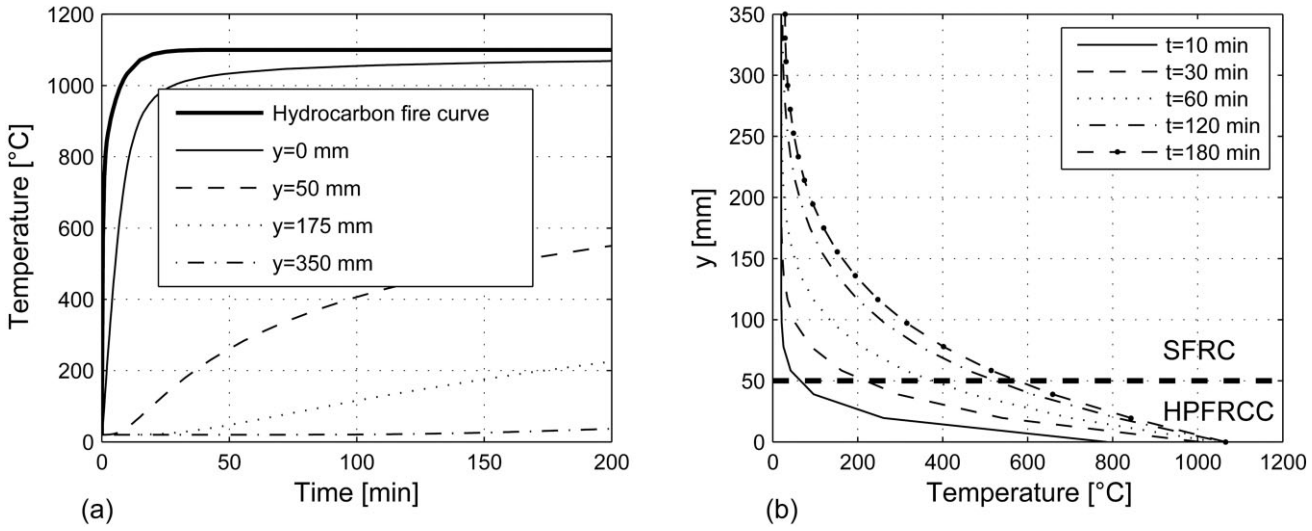

Fig. 6. Results of the 2D FE heat transfer analysis of the segment cross-section: a) temperature-time history imposed at the segment intrados and recorded at different depths *y* measured from the intrados of the tunnel segment, and b) temperature distribution along the segment cross-section for different fire exposure times (the horizontal dashed line represents the boundary of the HPFRCC external layer in the case of the layered solution)

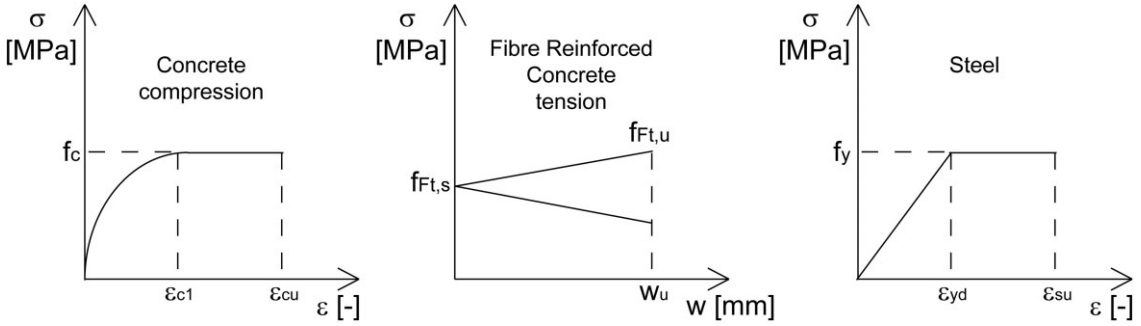

Fig. 7. Constitutive laws adopted for the different materials

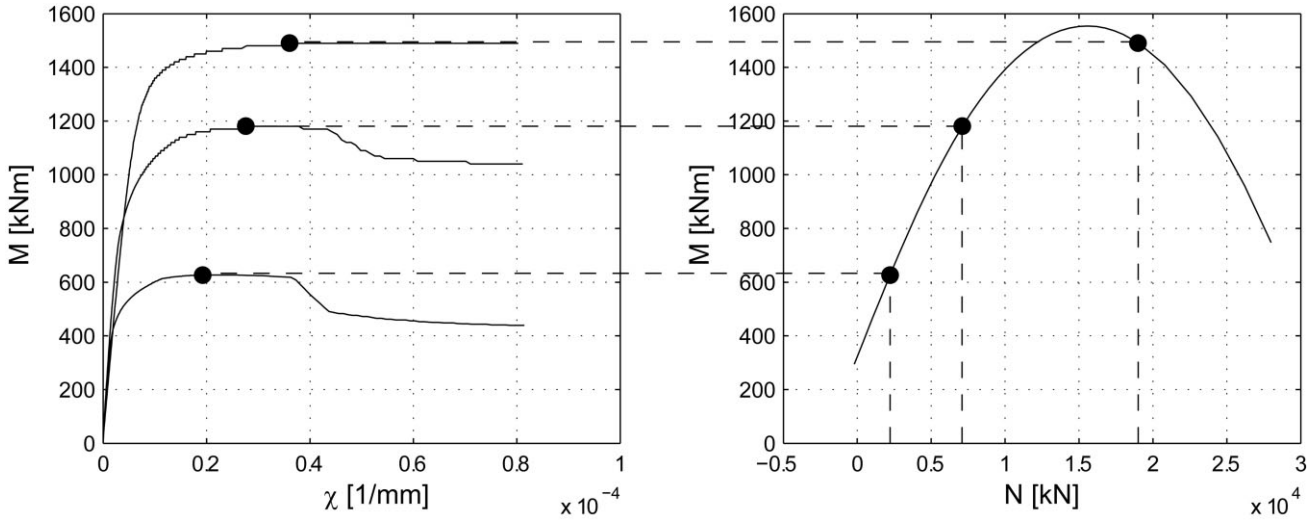

Fig. 8. *M-N* interaction diagram construction: example for three different points of the positive bending moment for the layered solution not exposed to fire

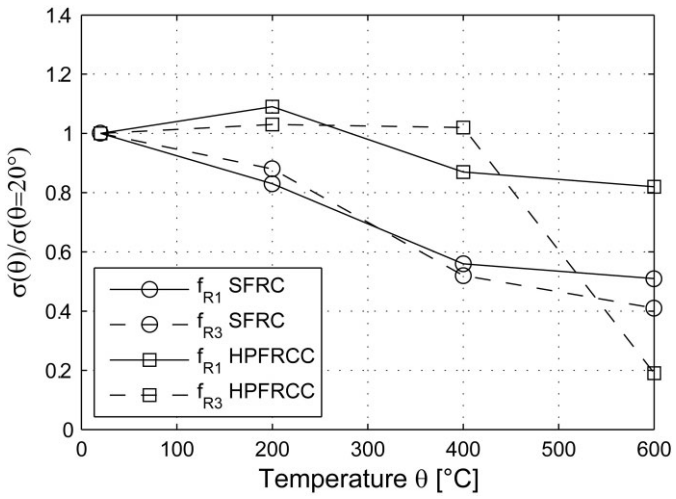

Fig. 9. Variation in the equivalent strengths f_{R1} and f_{R3} with temperature for SFRC and HPFRCC materials

60, 120 and 180 min) is presented in Fig. 10. In order to be able to see how the layered solution guarantees the improvement to the structural performance of the tunnel segment, a comparison between the resistant bending moment for $N = 0$ for the different fire exposure times considered is also shown (Fig. 11).

A second-order polynomial interpolation of the *M-N* diagram curve is used to cover all the axial force values, and a 5 % tolerance is used to define the failure of the cross-section. For example, considering the case of the layered solution for $t = 0$ min, cross-section failure takes place when the *M-N* actions combination falls within the shaded area of Fig. 12. Therefore, each point on the different *p-i* diagrams corresponds to a numerical simulation whose results satisfy the failure criterion related to the structural solution and the fire exposure time considered.

The same procedure is also applied to the joint cross-section, considering that no tensile stresses can be transmitted through the joint. It is worth noting that in all the situations investigated, the first cross-section that reaches the ULS is always in the segment cross-section. For this reason and for the sake of brevity, the joint *M-N* diagrams are not reported in this paper.

6.2 Results and discussion

The comparison of the structural responses of traditional RC and innovative fibre-reinforced layered solutions is presented in the following for tunnels subjected to internal explosion and pre-explosion fire actions. A previous preliminary study [22] has pointed out that the most restrictive failure mechanism is represented by the bending moment, as opposed to shear, in all the *p-i* diagram regions. For this reason, the shear limit state is disregarded in this study. The asymmetric cross-section resistances of both solutions compel us to build different *p-i* diagrams for positive and negative bending moments.

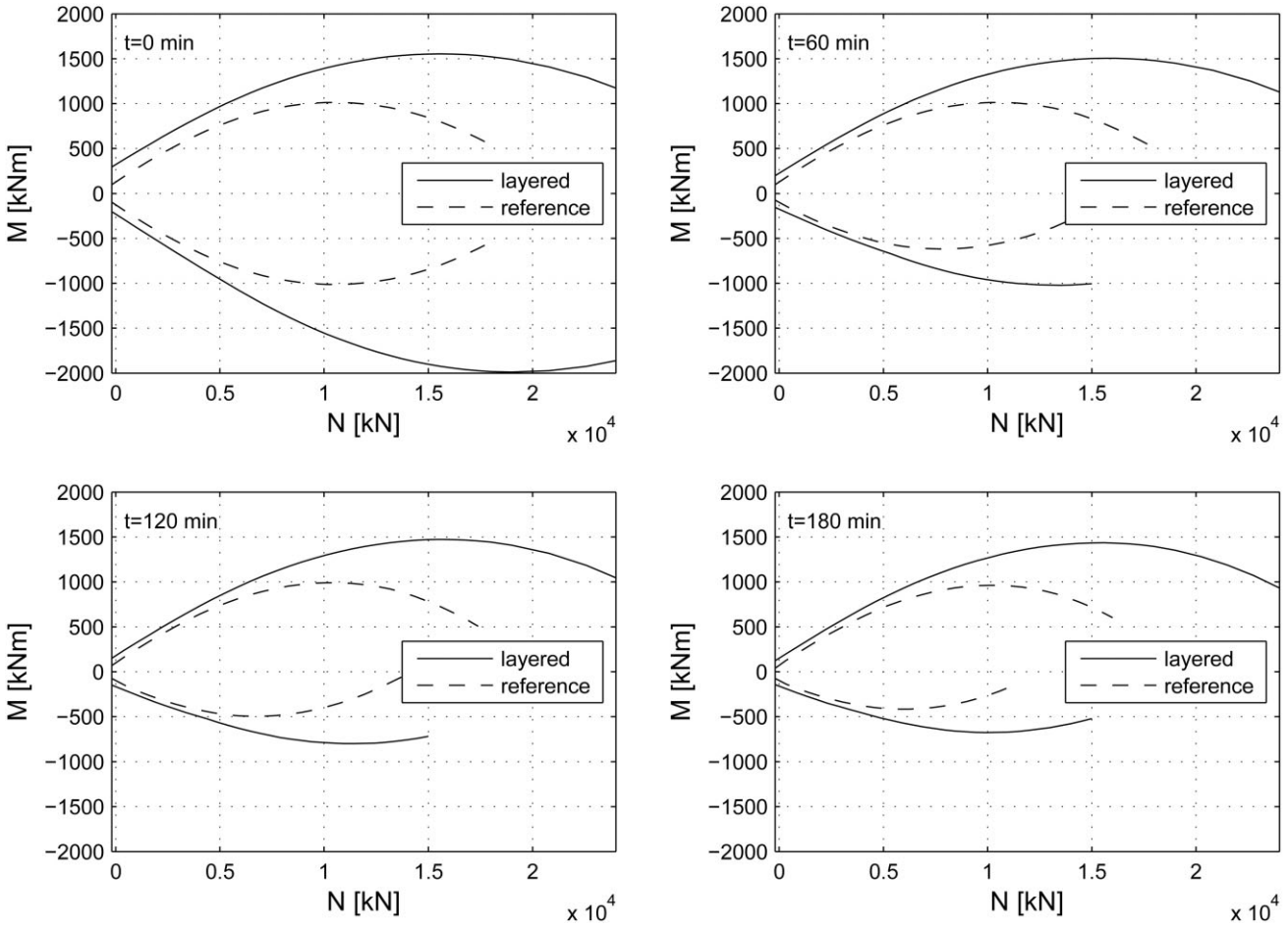

Fig. 10. Comparison between the *M-N* diagrams of the layered and reference solutions for the different exposure times considered

The *p-i* diagrams for positive (internal) and negative (external) bending moments are shown in Figs. 13a and 13b respectively for the case where no fire action precedes the internal explosion (t = 0 min). The composite layered solution shows a better performance in terms of both internal (Fig. 13a) and external bending moments (Fig. 13b); in fact, it is characterized by a wider safe zone in the graph. Moreover, Fig. 13 does not show intersection points between the traditional and innovative solution curves. This means that the layered solution performs better than the traditionally reinforced solution in all the loading domains (impulsive, dynamic and quasi-static).

Figs. 14, 15 and 16 show the *p-i* diagrams for positive (internal) and negative (external) bending moments for, respectively, the cases where a fire exposure of 60, 120 and 180 min precedes the internal explosion. The better performance of the fibre-reinforced layered solution compared with the traditional one is also confirmed in the case where the tunnel is subjected to pre-explosion fire actions.

A more concise way of comparing the two different tunnel structural solutions for different fire exposure times is presented in Table 3. The table lists the pressure and impulse asymptote values for different fire exposure times for the traditional and innovative structural solutions, and for both internal and external bending moments. The quantitative performance of the fibre-reinforced layered solution compared with the reference one is evaluated through a performance indicator η defined for both the asymptotes, for the internal and external limit states and for different fire exposure times as $\eta = (Lay. - Ref.)/Ref.$, where *Lay.* stands for layered solution values and *Ref.* for reference solution values. The performance indicator η reveals that the fibre-reinforced layered solution performs better than the traditional one for all the fire exposure times considered and for both positive and negative moments; the minimum and maximum relative increments of the layered solution compared with the traditional ones are 36.4 and 122 % respectively.

The innovative fibre-reinforced layered solution has a higher material cost with respect to the traditional one (+29 %). The material unitary costs considered for this economical evaluation were: SFRC 130 €/m^3, HPFRCC 500 €/m^3, plain concrete 80 €/m^3 and steel 1.5 €/kg. This higher cost of the layered solution is largely counterbalanced by the better performance a) under serviceability static loads (Fig. 11), b) in the case of fire action (Fig. 11) and c) in the case of internal explosion possibly preceded by fire action. Moreover, the reduced reinforcement ratio of the layered solution compared with the traditional one guarantees faster installation of the steel reinforcement with a reduction in the cost of labour. Despite this, the innovative solution is able to offer a mechanical reinforcement ratio ψ_s comparable with that offered by the traditional solution thanks to the positive contribution of HPFRCC in tension, as shown by Eqs. (7) and (8):

$$\Psi_{s-\mathrm{Ref.}} = \frac{f_{yd}A_s}{f_{cd}bd} = 0.029 \tag{7}$$

$$\Psi_{s-Lay.} = \frac{f_{yd}A_s + btf_{Ftu}^{HPFRCC}}{f_{cd}^{SFRC}bd} = 0.025 \tag{8}$$

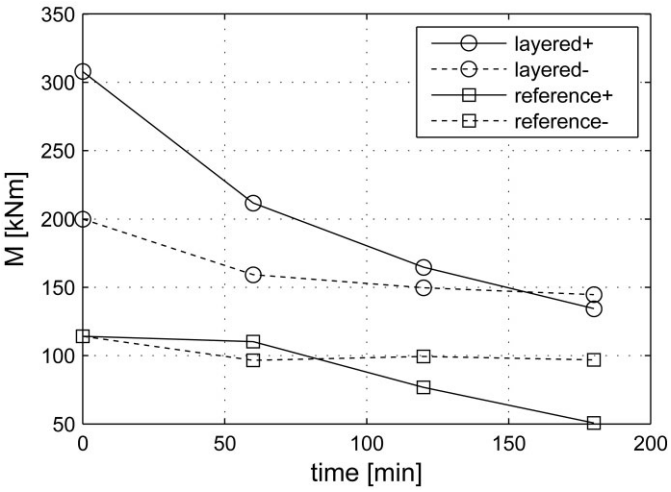

Fig. 11. How the resistant bending moment for axial force equal to zero (N = 0) varies with the fire exposure time

where:

A_s	steel area
f_{yd}	steel design yield stress
b	width of tunnel segment
d	distance between reinforcement centre and opposite edge
t	thickness of HPFRCC layer
f_{cd}^{SFRC}	SFRC design cylinder compressive stress
f_{Ftu}^{HPFRCC}	HPFRCC ultimate residual strength in tension

7 Conclusions

A design procedure based on a simplified FE model for underground tunnels subjected to internal explosion and pre-explosion fire conditions is proposed. The procedure provides a valuable tool for checking the structural safety of a tunnel in the case of an internal blast action possibly preceded by a fire accident. The case study is that of the metro line in Brescia, Italy. The tunnel considered has an internal diameter of about 8.15 m, is about 13.7 km long and is composed of six segments and a smaller key segment.

As a first step, the FE model was tested under static serviceability loads reproducing the soil pressure. Dynamic analyses were subsequently carried out in order to study the tunnel's response under internal blast loads in the form of pressure-impulse (*p-i*) diagrams. To this end, an ultimate limit state criterion based on eccentric flexural capacity (*M-N* interaction diagram) was introduced. At the same time, the limit state criterion is able to take into account the fire-blast interaction through a modification of the *M-N* diagram.

Two tunnel structural solutions are compared: a traditional solution where the lining section is made of RC and a new solution in which a layered precast tunnel segment is made of different fibre-reinforced cementitious composites.

The greater cost in terms of the materials used for the fibre-reinforced layered solution (about 29 %) compared with the traditional one is counterbalanced by:

a) the better performance under static loadings and in the case of fire, as clearly demonstrated in Fig. 11,

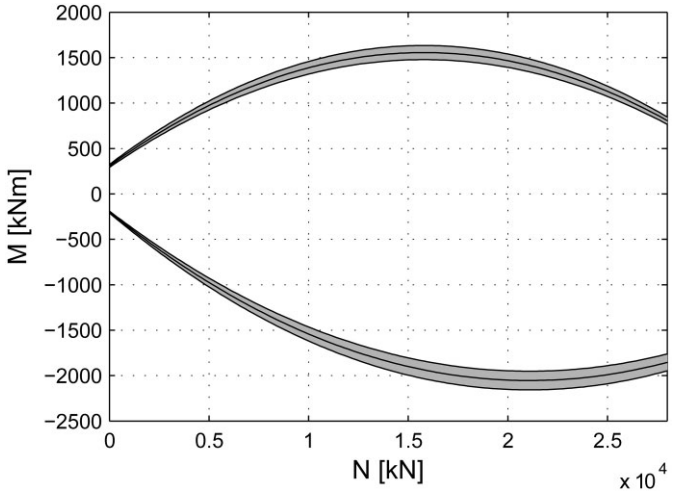

Fig. 12. Example of failure criteria adopted for the *p-i* diagram construction (layered solution for $t = 0$ min)

b) the better performance if subjected to internal explosion and in the case of pre-explosion fire actions, as discussed in the results section (Figs. 13–16 and Table 3), and
c) faster installation of the steel reinforcement in the production phase due to the lower reinforcement ratio, with a reduction in the cost of labour.

These results confirm the good potential for fibre-reinforced concrete composites in tunnel construction.

Finally, it is important to point out that the *p-i* diagrams derived in this work indicate that the tunnel reaches the ultimate limit state considered in one cross-section only. Since an underground tunnel is a statically indeterminate structure with a certain level of redundancy, the *p-i* diagrams do not correspond to the ultimate bearing capacity of the structure, but represent a conservative prediction.

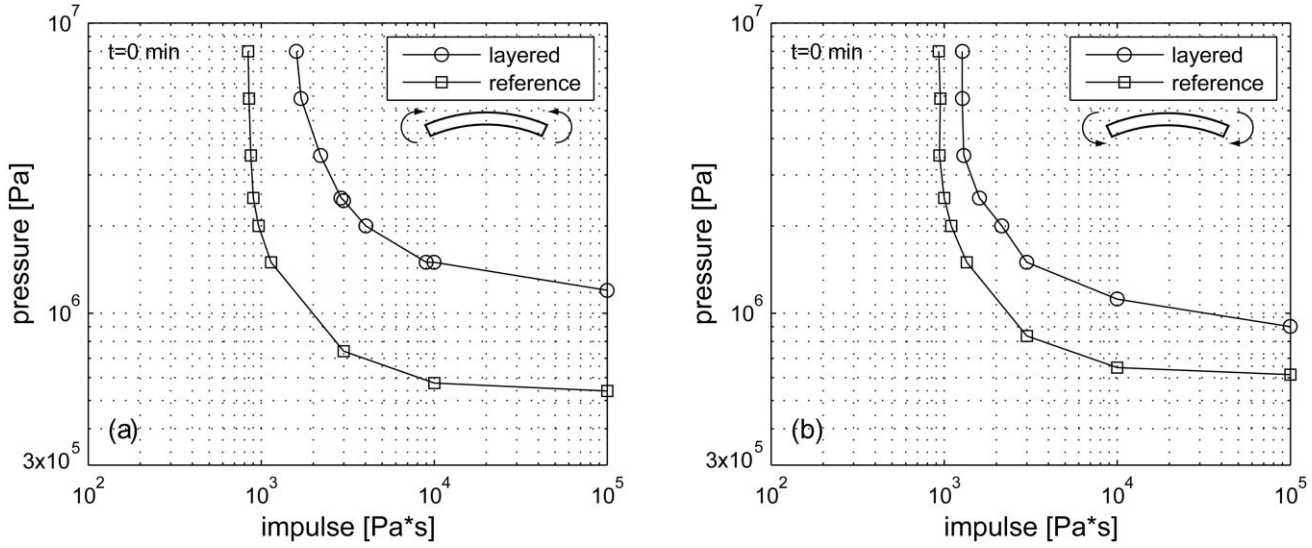

Fig. 13. Comparison of *p-i* diagrams for traditional RC and layered tunnel lining solutions without fire exposure: a) internal and b) external moment limit state

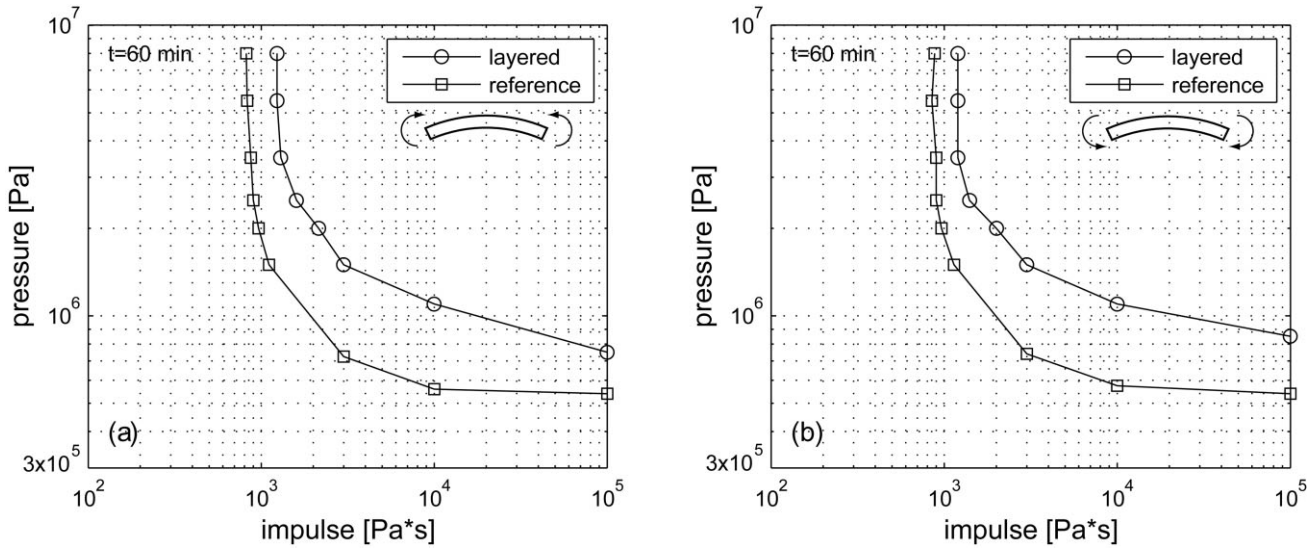

Fig. 14. Comparison of *p-i* diagrams for traditional RC and layered tunnel lining solutions for a fire exposure time of 60 min: a) internal and b) external moment limit state

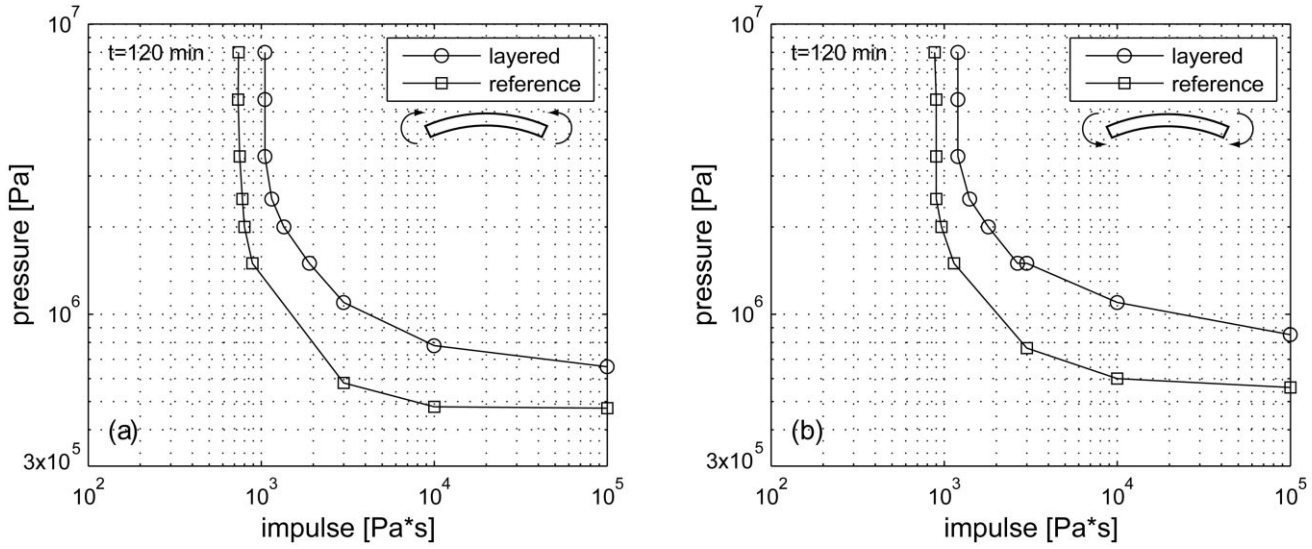

Fig. 15. Comparison of *p-i* diagrams for traditional RC and layered tunnel lining solutions for a fire exposure time of 120 min: a) internal and b) external moment limit state

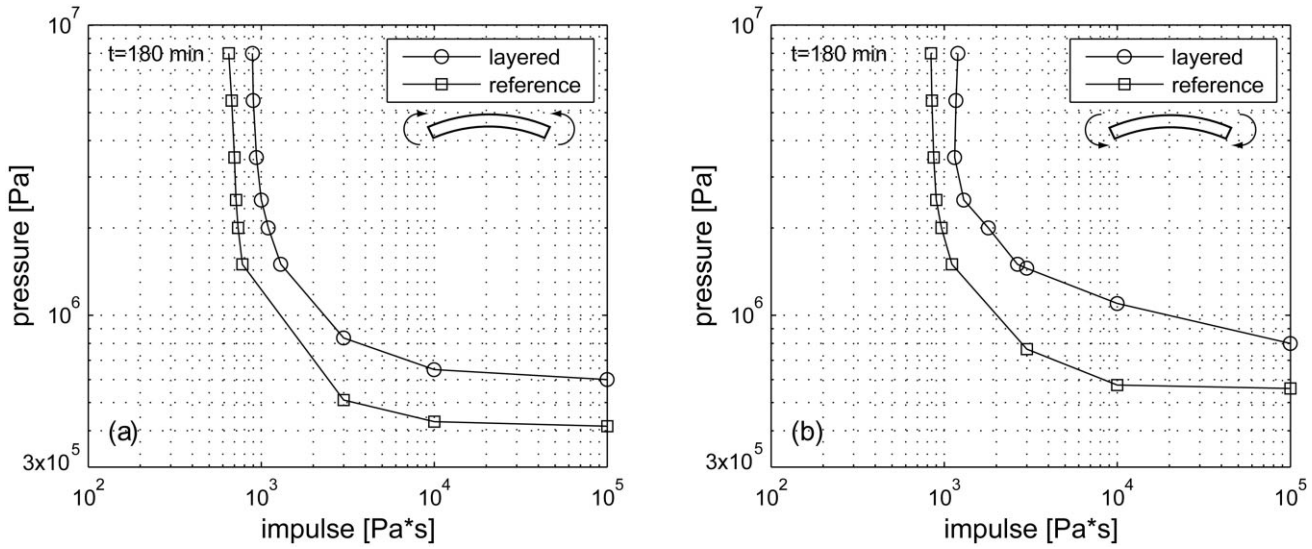

Fig. 16. Comparison of *p-i* diagrams for traditional RC and layered tunnel lining solutions for a fire exposure time of 180 min: a) internal and b) external moment limit state

Table 3 Impulse and pressure asymptote values for layered (Lay.) and reference (Ref.) structural solutions for different fire exposure times (η = (Lay. – Ref.)/Ref.)

Exp. Time (min)	Impulse asymptote (Pa · s)						Pressure asymptote (10^5 Pa)					
	M+			M–			M+			M–		
	Lay.	Ref.	η	Lay.	Ref.	η	Lay.	Ref.	η	Lay.	Ref.	η
0	1600	840	90.5 %	1270	930	36.6 %	12.0	5.4	122.2 %	9.0	6.15	46.3 %
60	1235	820	50.6 %	1200	880	36.4 %	7.5	5.4	38.9 %	8.5	5.4	57.4 %
120	1050	740	41.9 %	1200	880	36.4 %	6.6	4.75	38.9 %	8.5	5.6	51.8 %
180	890	650	36.9 %	1200	840	42.9 %	6.0	4.15	44.6 %	8.0	5.6	42.9 %

Acknowledgements

The research was supported financially by the European INTERREG IT/CH 2006_2013 project ACCIDENT ID 7629770, Measure 2.2. The authors wish to thank *Ren Huaping* for his help in FEM construction as a part of his MSc thesis in civil engineering at the Politecnico di Milano.

References

1. *Blom, C., van der Horst, E., Jovanovic, P.*: Three-dimensional structural analyses of the shield-driven "green heart" tunnel of the high-speed line south. Tunnelling and Underground Space Technology, 1999, 14, pp. 217–224.
2. *Chong, P., Tang, S. K., Lim, T., Sugawara, S., Furusono, T.*: Bored tunnel lining design in soft soils – a comparison between analytical and numerical analyses. In: Underground space for sustainable urban development, Proc. of 30th ITA-AITES World Tunnel Congress, 2004.
3. *Groeneweg, T.*: Shield driven tunnels in ultra high strength concrete. Master's thesis, Delft University of Technology, 2007.
4. *Tiberti, G.*: Concrete tunnel segments with combined traditional and fiber reinforcement: optimization of the structural behaviour and design aspects. PhD thesis, University of Brescia, 2009.
5 *Arnau, O., Molins, C.*: Experimental and analytical study of the structural response of segmental tunnel linings based on an in situ loading test. Part 2: Numerical simulation. Tunnelling and Underground Space Technology, 2011, 26, pp. 778–788.
6. *Cavalaro, S., Blom, C., Walraven, J., Aguado A.*: Structural analysis of contact deficiencies in segmented lining. Tunnelling and Underground Space Technology, 2011, 26, pp. 734–749.
7. *Winkler, B., Hofstetter, G., Lehar H.*: Application of a constitutive model for concrete to the analysis of a precast segmental tunnel lining. International Journal for Numerical and Analytical Methods in Geomechanics, 2004, 28, pp. 797–819.
8. *Sorelli, L., Toutlemonde, F.*: On the design of steel fiber reinforced concrete tunnel lining segments. In: 11th Intl. Conf. on Fracture, 2005.
9. *Baker, W., Cox, P., Westine, P., Kulesz, J., Strehlow, R.*: Explosion Hazards and Evaluation, Elsevier Scientific, 1983.
10. *Krauthammer, T., Astarlioglu, S., Blasko, J., Soh, T., Ng, P.*: Pressure impulse diagrams for the behavior assessment of structural components. International Journal of Impact Engineering, 2008, 35, pp. 771–783.
11. *Ma, G., Huang, X., Li, J.*: Damage assessment for buried structures against internal blast load. Structural Engineering and Mechanics, 2009, 32, pp. 301–320.
12. *Ma, G., Huang, X., Li, J.*: Simplified damage assessment method for buried structures against external blast load. Journal of Structural Engineering, 2010, 136, pp. 603–612.
13. *di Prisco, M., Beltrami, C., Bonalumi, P., Cadoni, E., Colombo, M., Ferrara, L., Martinelli, P.*: Hpfrc tunnel segments to mitigate the risk of exceptional loads. *fib* symp., Tel Aviv, Israel, 2013.
14. *Colombo, M., Martinelli, P., di Prisco, M.*: Layered high-performance concrete plates interacting with granular soil under blast loads: an experimental investigation. European Journal of Environmental and Civil Engineering, 2013, 17, pp. 1002–1025.
15. *fib* Model Code for Concrete Structures 2010. *fib*, International Federation for Structural Concrete, Ernst & Sohn, Berlin, 2013.
16. *Zani, G.*: High Performance Cementitious Composites for sustainable roofing panels. PhD thesis, Politecnico di Milano, 2013.
17. Abaqus Analysis User's Manual, version 6.12, vol. 2. Technical report, Simulia, 2012.
18. *Blom, C.*: Design philosophy of concrete linings for tunnels in soft soil. PhD thesis, Delft University of Technology, 2002.
19. *Tiberti, G., Plizzari, G.*: Tunnel linings of fiber reinforced concrete combined with traditional reinforcement. BEFIB symp., Chennai, India, 7th Intl. Symp. on Fibre Reinforced Concrete: Design and Applications, 2008.
20. *Tiberti, G., Plizzari, G.*: Parametric study on tunnel linings in fiber reinforced concrete combined with traditional reinforcement. In: Safe Tunnelling for the City and for the Environment, 2009.
21. *Janßen, P.*: Load capacity of segment joints. PhD thesis, Braunschweig University of Technology, 1983.
22. *Colombo, M., Martinelli, P., Huaping, R.*: Pressure-impulse diagrams for SFRC underground tunnels. In: Euro-C 2014 Computational Modelling of Concrete Structures, St. Anton am Alberg, Austria, 2014.
23. *Krauthammer, T., Bazeos, N., Holmquist, T. J.*: Modified SDOF analysis of RC box-type structures. J Struct Eng ASCE, 1986, 112, No. 4, pp. 726–44.
24. *Bonalumi, P.*: Soil-structure interaction under impulsive loading: Internal explosions in embedded pipes. PhD thesis, Politecnico di Milano, 2011.
25. EN 1992-1-2: Eurocode 2: Design of concrete structures – Part 1-2: General rules – Structural fire design. European Committee for Standardization, Brussels, 2004.
26. *Kooiman, A. G.*: Modelling steel fibre reinforced concrete for structural design. PhD thesis, Delft University of Technology, 2000.
27. *di Prisco, M., Ferrara, L., Colombo, M., Mauri, M.*: On the identification of sfrc constitutive law in uniaxial tension. In: *di Prisco, M., Felicetti, R., Plizzari, G.A.* (eds.), Proc. of 6th Symp. on Fibre-Reinforced Concrete, BEFIB, 2004, Bagneux, France, 2004, pp. 827–836.
28. *di Prisco, M., Colombo, M., Dozio, D.* (2013), Fibre-reinforced concrete in *fib* Model Code 2010: Principles, models and test validation. Structural Concrete, 14, 342–361. doi: 10.1002/suco.201300021
29. *Colombo, M., di Prisco, M., Felicetti, R.*: Mechanical Properties of Steel Fibre Reinforced Concrete Exposed at High Temperatures. Mater. Struct, 2010, 43, pp. 475–491.
30. *Caverzan, A., Colombo, M., di Prisco, M., Rivolta, B.*: High Performance steel fibre reinforced concrete: residual behaviour at high temperature. Mater. Struct, 2015, DOI: 10.1617/s11527-014-0401-9